JOURNAL OF ENVIRONMENTAL SCIENCES 87 (2020) 39–48

Available online at www.sciencedirect.com

ScienceDirect

www.elsevier.com/locate/jes

JES JOURNAL OF ENVIRONMENTAL SCIENCES

www.jesc.ac.cn

Preparation of hydrophobic hierarchical pore carbon–silica composite and its adsorption performance toward volatile organic compounds

Xiaoai Lu[1], *Junqian He*[1], *Jing Xie*[1], *Ying Zhou*[1], *Shuo Liu*[2], *Qiulian Zhu*[1], *Hanfeng Lu*[1,*]

1. *Research Institute of Catalytic Reaction Engineering, College of Chemical Engineering, Zhejiang University of Technology, Hangzhou 310014, China*

2. *Hangzhou Runxin Technology Co. Ltd, Hangzhou 310014, China*

ARTICLE INFO

Article history:
Received 2 March 2019
Revised 29 April 2019
Accepted 6 May 2019
Available online 13 May 2019

Keywords:
Hierarchical pores
Desorption
Stability
Volatile organic compounds (VOCs)

ABSTRACT

Carbon–silica materials with hierarchical pores consisting of micropores and mesopores were prepared by introducing nanocarbon microspheres derived from biomass sugar into silica gel channels in a hydrothermal environment. The physicochemical properties of the materials were characterized by nitrogen physical adsorption (BET), scanning electron microscopy (SEM), and thermogravimetric (TG), and the adsorption properties of various organic waste gases were investigated. The results showed that microporous carbon materials were introduced successfully into the silica gel channels, thus showing the high adsorption capacity of activated carbon in high humidity organic waste gas, and the high stability and mechanical strength of the silica gel. The dynamic adsorption behavior confirmed that the carbon–silica material had excellent adsorption capacity for different volatile organic compounds (VOCs). Furthermore, the carbon–silica material exhibited excellent desorption characteristics: adsorbed toluene was completely desorbed at 150°C, thereby showing superior regeneration characteristics. Both features were attributed to the formation of hierarchical pores.

Introduction

Volatile organic compounds (VOCs) are a class of complex organic pollutants that are ubiquitous in the atmosphere. Their pollution is mainly manifested in two aspects. First, most VOCs have toxicological properties and endanger human health (Wang et al., 2014b; Yi et al., 2009); second, some VOCs have strong photochemical reactivity and are capable of secondary conversion in the environment (Balan et al., 2017; Kamal et al., 2016). The photochemical reactions of VOCs dominate the process of photochemical smog formation, and they are essential to the generation of urban and regional ozone; moreover, the reactions are highly important precursors for ash weather (Chu et al., 2015).

To date, adsorption has become an important treatment process for volatile organic compounds by virtue of its simple operation and user-friendliness (Giraudet et al., 2006; Liu et al., 2018; Zhao et al., 2015). Activated carbon, with high adsorption capacity and broad adsorption spectrum, has consistently been of interest; however, it is characterized by several problems, such as difficulty in desorption and flammability (Böhme et al., 2005; Qiu et al., 2018). Some

* *Corresponding author. E-mail:* luhf@zjut.edu.cn (Hanfeng Lu).

https://doi.org/10.1016/j.jes.2019.05.003
1001-0742 © 2019 The Research Center for Eco-Environmental Sciences, Chinese Academy of Sciences. Published by Elsevier B.V.

studies have reported that composite materials can be used as adsorbents to control VOCs. Ojha et al. (2019) found that a graphitic carbon nitride (g-CN)/antimony-doped tin oxide (ATO) hybrid nanocomposite has good adsorption properties and excellent desorption behavior for many kinds VOCs. The application of carbon–silica composites has also been reported. Carbon–silica aerogel (CSA) composites have been synthesized from water glass and granulated activated carbon. Hydrophobic surfaces were obtained for the CSA composites by post-synthesis modification with trimethylchlorosilane (TMCS) and a subsequent ambient pressure drying procedure. The obtained CSA had good affinity toward aromatic molecules (Dou et al., 2011). A nanostructured porous carbon/silica composite was synthesized via a carbonization method by using a metal–organic framework (MOF)/silica composite as a sacrificial precursor, which showed excellent performance in removing a Congo Red pollutant from aqueous solution (Hu et al., 2016). Moreover, Twumasi et al. (2012) reported that a carbon–silica composite of 45% carbon content adsorbed more toluene than a carbon–silica composite of 32% carbon content. It can be seen that carbon–silica materials are very useful in VOC control. Therefore, it is worth looking for a simpler and more efficient method to prepare carbon–silica composites.

Silica gel is a non-conductive and strongly hydrophilic porous material with a high specific surface area. Silica gel is extremely versatile and can be made into an excellent adsorbent material for volatile organic compounds via different methods of modification (Wang et al., 2016b). Two major obstacles hinder wider use of silica gel in practical application: namely, its considerable hydroxyl content and large pore size. Many applications of silica gels and studies on their hydrophobicity and pore modification have been reported previously. Examples include introducing carbon from rice husks to prepare a micron-sized porous C/SiO_2 composite for electrochemical applications via a simple carbonization process (Cui et al., 2017). The produced lithium ion battery anode material had a high discharge specific capacity, good electron conductivity, and excellent cycle stability due to its porous structure. Moreover, reports have described using glucose and tetraethyl orthosilicate (TEOS) via carbonization and a gel procedure to synthesize a silica–carbon–silica core-shell composite for precious metal loading. The unique core-shell spherical composite has a significant chemical effect on the loading of different catalyst materials. The core-shell sphere can be further processed to form a hollow carbon capsule or a double silicon sphere, both of which are precious metal carriers with great prospects (Wan et al., 2008). Hydrophobic properties are controlled by two factors, namely, surface free energy and roughness. Surface free energy is related to all the components of the surface, and silica gel is hydrophilic due to the presence of numerous hydroxyl groups in its pores. Previous papers have reported that *p*-divinylbenzene (PDVB) can be used to modify silica gel into a superhydrophobic material (Lu et al., 2013). The first step is replacing the hydroxyl groups of the silica gel with alkyl groups using a silane coupling agent to improve the grafting channels. Afterward, PDVB is introduced in an extremely favorable environment to result in excellent modification. The prepared sample has super-hydrophobicity and high adsorption capacity, thereby giving it broad prospects for treating VOCs. This approach represents another way to use carbon nanotubes to increase the surface roughness of a smooth graphene surface (Wang et al., 2017), in order to synthesize a carbon nanotube-graphene gel equipped with desirable hydrophobic properties (Lu et al., 2017).

Current studies focus on the initial stage of the combination of silica gel and activated carbon, but do not apply these methods for treating organic waste gas. Additionally, the effect of carbon–silica material on the adsorption of organic waste gas is highly significant, but further in-depth research is needed to improve the combination of the resulting pores, which is highly conducive to the adsorption and desorption of organic waste gas. The formation of hierarchical pores is not only beneficial to adsorption but also causes organic molecules to be desorbed efficiently under the influence of two forces, namely, self-desorption energy and the interaction between mesopores and micropores.

Motivated by the above discussion, we report the preparation of a carbon–silica adsorbent via hydrothermal carbonization, with an aim to creating the morphology of graded pores in order to improve the adsorption capacity and hydrophobicity of the silica material, and obtain excellent desorption characteristics. In the present study, biomass or a high-molecular-weight polymer was used as the carbon source, and the precursor was synthesized by using a hydrothermal method. Afterward, heat treatment was conducted to obtain a carbon–silica material. Various techniques were used to study the morphology and surface properties of the materials, and the adsorption and desorption behaviors for volatile organic compounds were evaluated.

1. Materials and methods

1.1. Materials

Mesoporous spherical silica gel (Qingdao Meigao Group Co., Ltd., China) was used as a carbon–silica material skeleton, 3–5 mm particles; dodecyl trimethoxysilane (97%, Sinopharm Chemical Reagent Co., Ltd., China) and absolute ethanol (99.7%, Anhui Ante Food Co., Ltd., China) were used as a silica hydrophobic modification reagent. Moreover, sucrose (Guangdong Guanghua Chemical Co., Ltd., China) was used as a carbon source. All chemicals were used as received and without further purification.

1.2. Preparation of adsorbent

Hydrophobization process: silica gel (8 g) was placed in a 50 mL round-bottom flask that contained ethanol (10 g) and dodecyltrimethoxysilane (1 g). Reflux condensation was conducted for 10 hr in a constant temperature water bath (85°C), and the product was filtered and dried in an oven (110°C).

Carbonization process: preparing sucrose solution (50%): sucrose (8 g) was dissolved in deionized water (8 g), stirred with a glass rod until completely dissolved, and the silicified silica gel was placed in the sucrose solution

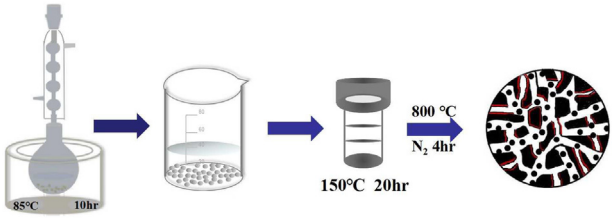

Fig. 1 – Schematic diagram of the preparation process of carbon–silica materials.

for approximately 10 hr. After filtration, the mixture was poured into a Teflon-lined stainless-steel autoclave (20 mL), which was heated in a crystallization tank (150°C, dwell time 20 hr). After the autoclave was naturally cooled, the removed sample was washed several times with deionized water until clean, and dried at 110°C for nearly 2 hr. The sample was placed in a baking furnace (50 mL/min N_2, heating rate of 5°C/min from 25 to 800°C, constant temperature 4 hr) to obtain a carbon–silica composite adsorbent. The specific experimental process is shown in Fig. 1.

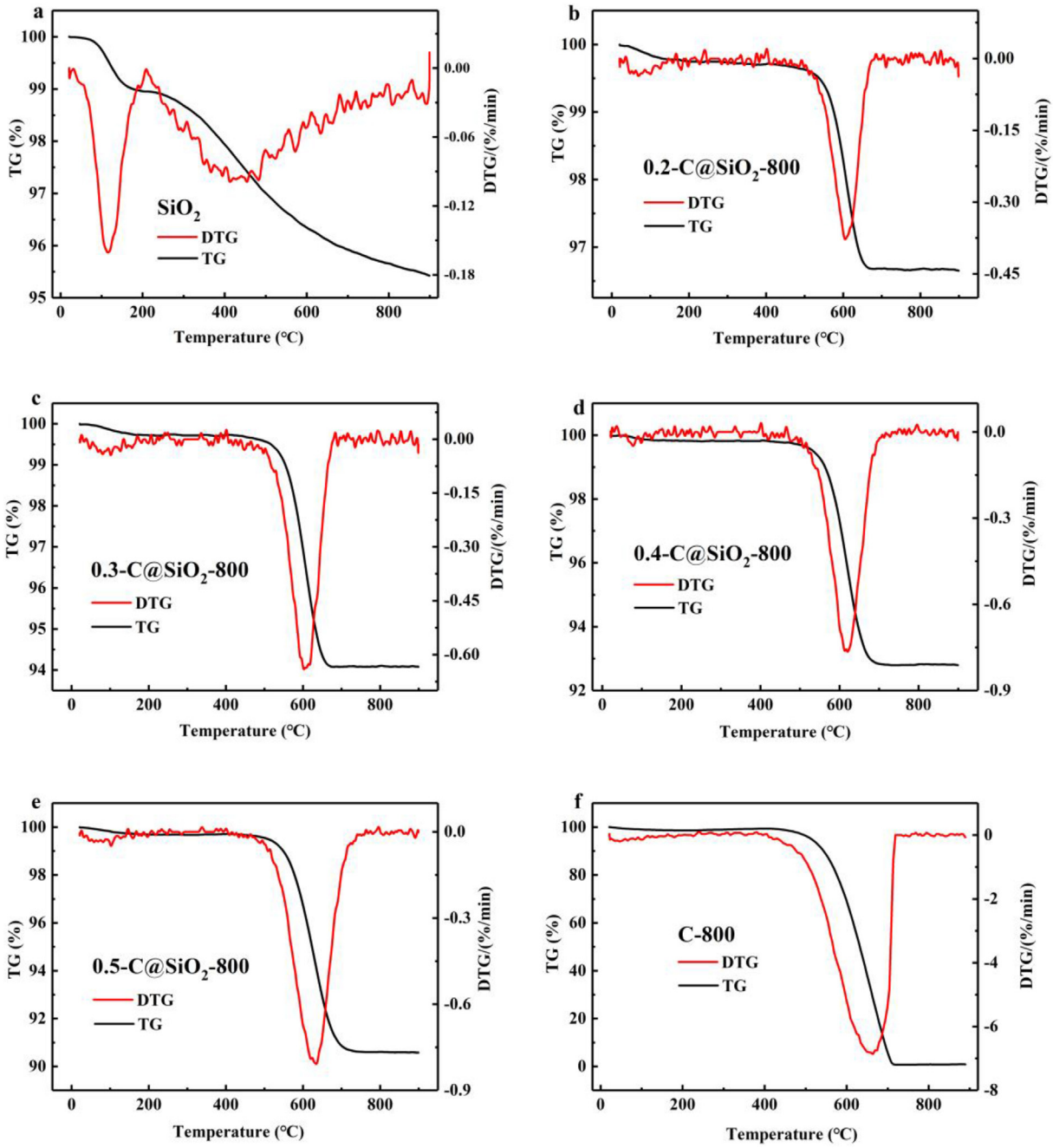

Fig. 2 – Thermogravimetric (TG) curves of (a) SiO_2, (b) 0.2-C@SiO_2-800, (c) 0.3-C@SiO_2-800, (d) 0.4-C@SiO_2-800, (e) 0.5-C@SiO_2-800, and (f) C-800. *X*-C@SiO_2-800: carbon–silica materials prepared with different sucrose concentrations (*X* = 0.2, 0.3, 0.4, and 0.5); C-800: the biomass carbon (50% sucrose concentration); SiO_2: the original silica gel; DTG: derived thermogravimetric.

Nomenclature: X-C@SiO_2-800 represents carbon–silica materials prepared with different sucrose concentrations, and X is the mass concentration of sucrose (20%, 30%, 40%, and 50%). The biomass carbon (50% sucrose concentration) is named C-800, the calcined raw silica gel is named SiO_2-800, and the original silica gel is SiO_2.

1.3. Characterization

The porosity of all the samples was measured by N_2 adsorption/desorption isotherms at −196°C in a volumetric analyzer (3-Flex, Micromeritics, USA). Before the experiment, the sample was degassed at 100°C for 12 hr in a vacuum (10^{-4} Torr). The specific surface area, pore volume, and pore diameter were calculated by using the Brunauer–Emmett–Teller (BET) theory and Barrett–Joyner–Halenda (BJH) method (Gong et al., 2018; Kiciński et al., 2017). Thermogravimetric (TG) results of all the samples were analyzed using a instrument (STA409PC, NETZSCH, Germany, 10°C/min from 20 to 900°C, air 50 mL/min). Based on the TG curve, we obtained the differential derived thermogravimetric (DTG) curves. The water contact angle (WCA) of the sample was measured via electro-optics by using a theta optical tensiometer, and electro-optics with a closed-circuit television camera connected to a computer (OCA-20, Dataphysics, Germany). One drop of distilled water (3 μL) was dropped onto the surface of the sample. The measures were conducted thrice, and the average value was recorded. The morphology and elemental analyses of the sample were obtained via scanning electron microscopy (SEM, S4800, Hitachi, Japan) and energy dispersive spectroscopy (EDS, S4800, Hitachi, Japan), respectively.

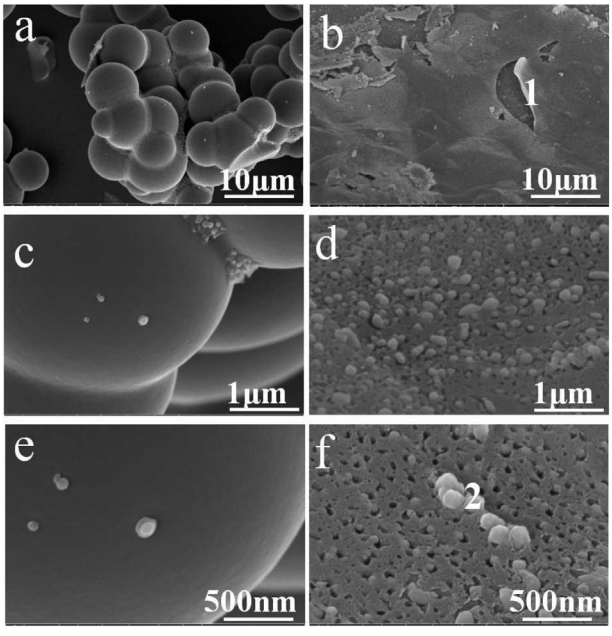

Fig. 3 – (a, c, e) Scanning electron microscopy (SEM) images of C-800 and (b, d, f) 0.5-C@SiO_2-800.

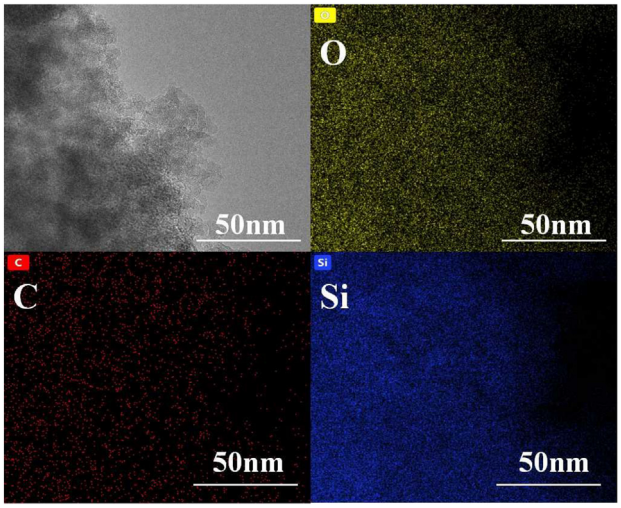

Fig. 4 – Transmission electron microscopy (TEM) images of 0.5-C@SiO_2-800 and corresponding elemental mappings.

1.4. Adsorption performance test

Gaseous organic compounds were generated by passing air through a bubbler that contained the liquid organic matter at 0°C, and the flow volume was regulated by a mass flow controller, which was transferred to a buffer bottle, and diluted with further air to the desired concentration. Another bubbler that contained distilled water (to control the humidity of the VOC gas) was placed in a constant temperature water bath (30°C). The three-way gas was collected in the sample column (10 mm in diameter, 20 mm in height) in a U-shaped reaction tube, which was packed with approximately 1 g of adsorbent, and thermostatted in a 30°C water bath. The gas hourly space velocity (GHSV) was 10,000 mL/(hr·g), and the exhaust gas was detected by using a gas chromatograph equipped with a flame ionization detector (7890, Agilent, USA).

A glass tube (5 cm in diameter) filled with water (2.5 cm in height) was placed in a constant temperature water bath (30°C). The water bath was placed under the electronic balance from whose hook hung a cube (4 cm^3 in volume) made of fine wire mesh with nylon wire. Carbon–silica adsorbent (0.5 g) was placed in the cube, which was hung about 2 cm above the water surface in the glass tube. The electronic balance was

Table 1 – Elemental analysis.

Element		Mass percentage (wt.%)	Atom percentage (at.%)
C	a	51.89	61.87
	b	68.17	75.81
O	a	35.32	31.61
	b	25.19	21.03
Si	a	12.79	6.52
	b	6.65	3.16

a and b represent carbon membranes and carbon spheres, respectively.

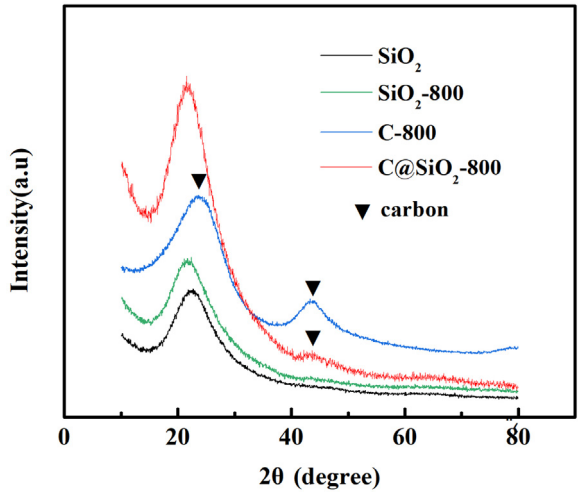

Fig. 5 – X-ray diffraction (XRD) of SiO_2, SiO_2-800, C-800 and C@SiO_2-800. SiO_2-800: the calcined raw silica gel.

linked to the computer, and the balance data were recorded directly in the computer. The data were recorded once every half minute, and the entire process lasted 6 hr.

2. Results and discussion

2.1. Determination of carbon content

Fig. 2 shows the TG and corresponding DTG curves of SiO_2, 0.2-C@SiO_2-800, 0.3-C@SiO_2-800, 0.4-C@SiO_2-800, 0.5-C@SiO_2-800, and C-800. As seen in Fig. 2, approximately 1% mass loss occurs at approximately 100°C, which is attributed to the molecular water adsorbed on the silica surface. The loss of weight in the temperature range 100–200°C is due to silica impurities or internal pyrolysis (Yu et al., 2018). As shown in Fig. 2b, c, d and e, the same weight loss peaks occurred at 500–700°C, and C-800 lost 100% mass especially, thereby indicating that the peaks of the carbon–silica materials were inferred to derive from the biomass carbon. Fig. 2 shows that high sucrose concentration increased the carbon content, thereby indicating that biomass carbon was successfully loaded in the silica pores, and the mechanical strength also showed a 34.6% increase, as illustrated in Appendix A Fig. S1.

2.2. Morphology and surface properties of the sample

The SEM and transmission electron microscopy (TEM, Tecnai G2F30, FEI, Netherland) images reveal differences between 0.5-C@SiO_2-800 and C-800 (Figs. 3 and 4), and their morphologies were clear and comparable. A membrane was produced in the porous surface of sample 0.5-C@SiO_2-800 in Fig. 3b (Chen et al., 2017), which consisted of a high amount of carbon and low amount of silica, from the EDS results Table 1a. The microcosmic morphology of the biomass carbon appears spherical (Fig. 3a). Furthermore, Fig. 3f shows spherical particles, which are recognized as activated carbon from Table 1b. These figures indicate that some activated carbon grew in the orifice perfectly, and their size was controlled by the silica pores (Cavaliere et al., 2018). Fig. 4 shows the C and Si distributions, and that they are intertwined on the microscopic scale.

X-ray diffraction (XRD, X' Pert Pro, PANalytical, Netherland) was used to determine the structure of samples. Fig. 5 shows the XRD patterns of SiO_2, SiO_2-800, C-800 and 0.5-C@SiO_2-800. A broad peak between 20 and 27°, centered at 23°, can be assigned to the overlap between the amorphous C and amorphous SiO_2 peaks in all samples (Cui et al., 2017). In addition, the peak around 43° is attributed to the amorphous C in C-800 (Yao et al., 2011; Zhao et al., 2017), and there is similar weak peak in C@SiO_2-800. Therefore, the evidence showed that carbon materials were loaded successfully in SiO_2.

As shown in Fig. 6b, when the relative pressure reached approximately 0.6, 0.5-C@SiO_2-800 exhibited a type IV isotherm 442.5 cm^3/g, which is a typical characteristic of mesoporous materials; whereas C-800 exhibited type I isotherms, and these parameters are typical of microporous

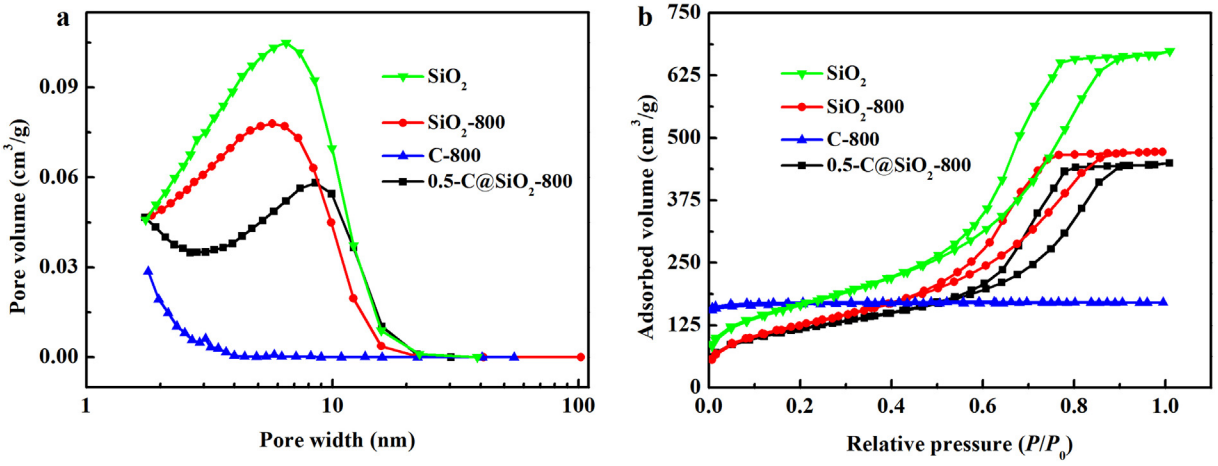

Fig. 6 – (a) Pore size distributions (PSDs) and (b) the N_2 adsorption–desorption isotherms of SiO_2, SiO_2-800, C-800 and 0.5-C@SiO_2-800.

Table 2 – Pore structure parameters of SiO_2, SiO_2-800, C-800 and 0.5-C@SiO_2-800.

Sample	Pore size (nm)	Pore volume (cm^3/g)	S_{BET} (m^2/g)
SiO_2	6.92	1.03	596
SiO_2-800	6.36	0.73	460
C-800	2.05	0.26	514
0.5-C@SiO_2-800	6.64	0.69	416

S_{BET}: specific surface area.

materials. Fig. 6a shows that all samples except C-800 display pore size distributions (PSDs) with most pores having sizes between 0 and 50 nm, and this result indicates that all samples have mesoporous characteristics. Furthermore, 0.5-C@SiO_2-800 shows small peaks of pores with sizes less 2 nm, such as C-800, which only manifests in the two samples having micropores. Afterward, hierarchical pores formed in 0.5-C@SiO_2-800, which were attributed to activated carbon growing in the mesopores of silica. The above results are clearly consistent with the pore structure parameters calculated from the N_2 isotherms. Table 2 shows the porosity characteristics of all samples.

To investigate the surface properties of the carbon–silica composite materials, the water contact angle (WCA) of the samples was tested (Zhao et al., 2017). As shown in Fig. 7, the water contact angle of SiO_2 was 25.8° because of the numerous hydroxy groups in the pores, whereas that of SiO_2-800 was increased to 89.6° due to the disappearance of hydroxy groups at 800°C. The water contact angle of the biomass carbon was 146.9°, and its surface roughness improved its hydrophobicity. The biomass carbon caused the water contact angle of 0.5-C@SiO_2-800 to reach 106.4°, which was significantly higher than that of SiO_2 (CA = 25.8°). This result showed that biomass carbon was successfully grown in the SiO_2 pores, thereby indicating that the roughness of 0.5-C@SiO_2-800 increased on

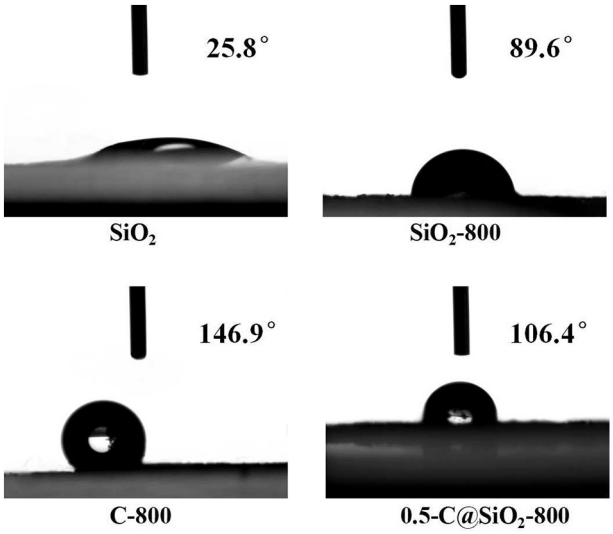

Fig. 7 – Water contact angle of SiO_2, SiO_2-800, C-800, 0.5-C@SiO_2-800.

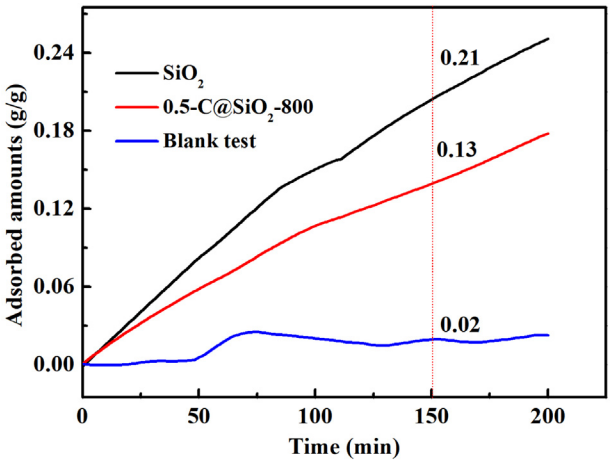

Fig. 8 – Static adsorption of SiO_2, 0.5-C@SiO_2-800 and blank test.

account of silanization and introduction of biomass carbon, which both increased the hydrophobicity of 0.5-C@SiO_2-800.

For further test the hydrophobic properties of 0.5-C@SiO_2-800, the static adsorption of water in the samples was tested. As seen in Fig. 8, compared with SiO_2, 0.5-C@SiO_2-800 has a certain degree of hydrophobicity. The adsorption capacity of SiO_2. 0.5-C@SiO_2-800 and the blank test were 0.21, 0.13, and 0.02 g/g in the environment of evaporated water at 30°C for 150 min. This result indicated that the adsoption capacity of 0.5-C@SiO_2-800 was nearly half than that of SiO_2, thereby exhibiting the highest water vapor adsorption capacity due to the high density of surface hydroxyls. This result revealed that the hydrophobicity of 0.5-C@SiO_2-800 was improved, which was aligned with our objective (Wang et al., 2014a, 2016a).

2.3. Dynamic adsorption and desorption performance

2.3.1. Comparison of adsorption property

Fig. 9 describes the breakthrough curves of toluene during adsorption on SiO_2, SiO_2-800, 0.2-C@SiO_2-800, 0.3-C@SiO_2-800, 0.4-C@SiO_2-800, and 0.5-C@SiO_2-800. The breakthrough time and dynamic adsorption capacity of toluene on these samples are listed in Table 3. The dynamic adsorption can be divided into three stages: adsorption saturation zone, adsorption mass transformation zone, and adsorption breakthrough zone (Zhang et al., 2018). At the beginning of adsorption, the outlet gas concentration of toluene was approximately 0, from the dynamic adsorption curve of the carbon–silica materials, whereas SiO_2-800 and SiO_2 were penetrated immediately under high humidity. These results indicated that they preferentially adsorbed water vapor, whereas the carbon–silica materials preferentially adsorbed toluene. As the adsorption continued, the mass transfer zone moved up gradually as adsorption time increased and reached the top of the carbon–silica materials. In the third stage, the concentration at the outlet gradually approached that of the inlet concentration. As shown in the diagram, increased sucrose concentration

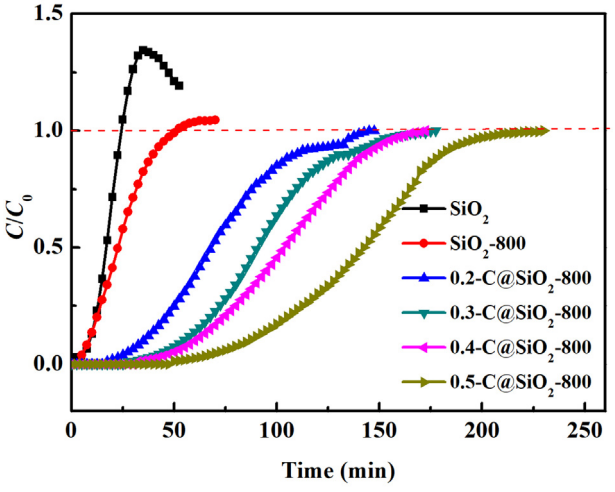

Fig. 9 – Adsorption characteristics of toluene on six samples. Adsorption conditions: relative humidity (RH) = 80%, C_0 = 1000 mg/m^3, temperature (*T*) = 30 °C, and GHSV = 10,000 mL/(hr·g). *C*: outlet toluene concentration.

and increased carbon content improved the adsorption effect. This result was in good consistency with the above description. The increase of biomass carbon significantly increased the adsorption capacities of the carbon–silica material. The data in Table 3 show that the result was clear, which proved that the adsorption performance of carbon–silica material was secondary to the combination of SiO_2 and activated carbon.

2.3.2. Water vapor influence

The above performance comparison confirmed that increasing the sucrose concentration and carbon content improves the adsorption performance. Therefore, the sucrose concentration was 50%, as an example. The dynamic adsorption experiments of toluene on four samples under dry conditions and relatively humid conditions (80% relative humidity (RH)) are shown in Fig. 10. The figure shows that SiO_2 is penetrated almost immediately in a high-humidity environment. In this test, only 0.5 g activated carbon was loaded because it would otherwise require a long time, whereas the remaining samples had 1 g. The adsorption amounts in Table 4 are calculated in the same proportion and can be compared. The figure shows that the presence of activated carbon provided a large advantage in adsorption capability, but the adsorption performance of 0.5-C@SiO_2-800 increased considerably compared with SiO_2; moreover, the difference in adsorption amounts can be clearly found in Table 4. The carbon content column shows that if the carbon amount of the carbon–silica material is equivalent to the carbon amount of the activated carbon, the amount of adsorption obtained via conversion is higher than that of activated carbon with the same carbon content. Therefore, the adsorption of toluene by the carbon–silica material was not only affected by the carbon in the silica gel pores, but was also the effect of the combination of the activated carbon microspheres and silica gel. This effect, combined with morphology and other advantages, gives these materials greater performance in the application of VOC emissions abatement under high humidity than activated carbon.

2.3.3. Adsorption of other VOCs

Toluene is typical of many VOCs, and the adsorption performance of carbon–silica materials on other organic waste gases was investigated in this paper. Toluene represents aromatic hydrocarbon organic waste gas, ethyl acetate represents oxygen-containing organic waste gas, and acetone represents ketone organic waste gas (Zaitan et al., 2016). Moreover, ethanol represents small-molecule organic waste gas for the purposes of adsorption evaluation. Fig. 11a shows that the carbon–silica materials caused an adsorption effect on the selected organic waste gases. The adsorption effects of ethanol, toluene, and ethyl acetate were the most significant. The pores were not only suitable for oxygen-containing organic substances, but also highly suitable for aromatic hydrocarbon organic waste gas and small-molecule organic substances. However, SiO_2 showed hardly any adsorption performance for the deadly types of organic waste gases, as seen in Appendix A Fig. S2.

An excellent adsorbent not only shows good adsorption performance but also exhibits efficient desorption (Chu et al., 2016). Fig. 11b shows a comparison of the thermal desorption of VOCs from the carbon–silica material and the

Table 3 – Toluene adsorption data of six samples.

Sample	Breakthrough time (min)	Breakthrough adsorption (mg/g)	Saturated time (min)	Saturated adsorption (mg/g)	Carbon content
SiO_2	2.5	0.42	52.5	1.63	0
SiO_2-800	5	0.83	70	3.80	0
0.2-C@SiO_2-800	17	2.90	147	11.76	3.09%
0.3-C@SiO_2-800	27	4.56	177	15.26	5.66%
0.4-C@SiO_2-800	32	5.39	172	17.00	7.02%
0.5-C@SiO_2-800	50	8.30	230	22.91	9.10%

Adsorption conditions: RH = 80%, inlet toluene concentration (C_0) = 1000 mg/m^3, and gas hourly space velocity (GHSV) = 10,000 mL/(hr·g).

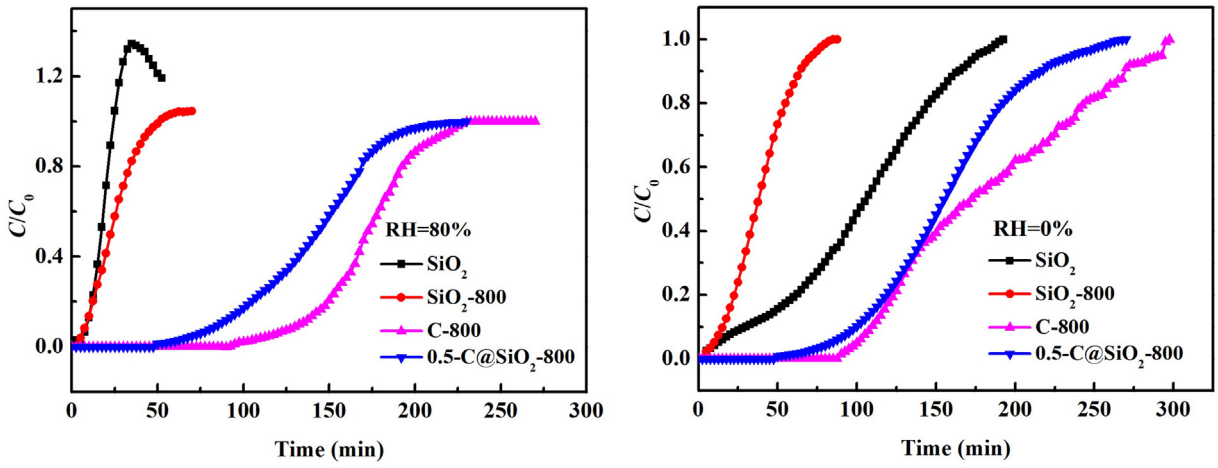

Fig. 10 – Adsorption curves of SiO_2, SiO_2-800, C-800, 0.5-C@SiO_2-800 of toluene under different humidity. Adsorption conditions: C_0 = 1000 mg/m^3, T = 30°C, and GSHV = 10,000 mL/(hr·g).

Table 4 – Adsorption capacity of SiO_2, SiO_2-800, C-800, 0.5-C@SiO_2-800.

Sample		Breakthrough time (min)	Breakthrough adsorption (mg/g)	Saturated time (min)	Saturated adsorption (mg/g)	Carbon content
SiO_2	a	2.5	0.42	52.5	1.63	0
	b	5	0.83	192.5	17.09	
SiO_2-800	a	5	0.83	70	3.80	0
	b	2.5	0.41	87.5	6.47	
C-800	a	95	78.54	270	155.70	100%
	b	90	29.49	297.5	60.76	
0.5-C@SiO_2-800	a	50	8.31	230	22.91	9.10%
	b	50	8.30	270	25.91	

a and b: adsorption data of SiO_2, SiO_2-800, C-800 and 0.5-C@SiO_2-800 toward toluene when RH = 80% and RH = 0% are obtained, respectively.

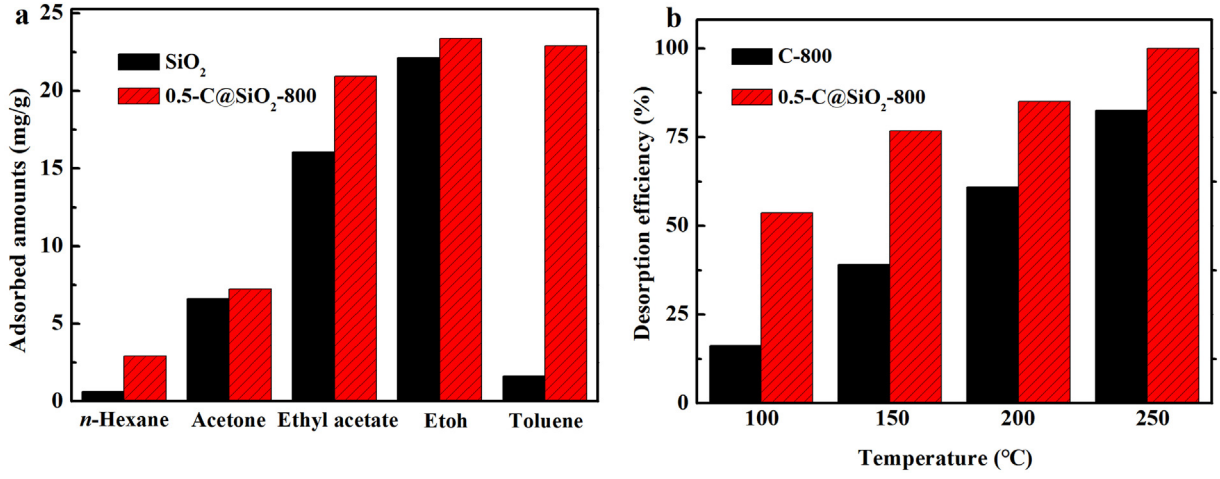

Fig. 11 – (a) Comparison of adsorption amounts between SiO_2 and 0.5-C@SiO_2-800 for different VOCs and (b) comparison of desorption efficiency of toluene between C-800 and 0.5-C@SiO_2-800. Adsorption conditions: RH = 80%, C_0 = 1000 mg/m^3, T = 30°C, and GHSV = 10,000 mL/(hr·g). Etoh: ethanol.

activated carbon sample via TG analysis (the temperature was raised from 30°C at 10°C/min to 250°C, dwelling 1 hr). The weight loss rate of activated carbon only reached approximately 60% above 200°C, and 0.5-C@SiO_2-800 was desorbed almost absolutely at 150°C, as shown in Appendix A Fig. S3. Compared with activated carbon, the advantage of carbon–silica materials in terms of desorption efficiency was clear, as seen in Fig. 11b. In the case of different temperatures, the desorption rate of activated carbon was not synchronized with the efficiency of 0.5-C@SiO_2-800. Therefore, 0.5-C@SiO_2-800 is highly valuable for recycling. The reason may be that activated carbon is highly difficult to desorb because of its narrow pore size, and in carbon–silica materials, the biomass carbon microspheres growing in silica gel channels retain the mesoporous effects of SiO_2 during desorption, thereby facilitating desorption and expediting the desorption under relatively low temperatures. Combining all the advantages and disadvantages, 0.5-C@SiO_2-800 was shown to very environmentally friendly, and may be utilized immediately. In terms of adsorption, VOCs can be adsorbed not only by the pores of the SiO_2 but also by the biomass carbon microspheres in the pores. Compared with the desorption efficiency of activated carbon, the desorption efficiency of carbon–silica is more efficient and rapid (Kuntasal et al., 2005).

3. Conclusions

Hydrophobic carbon–silica materials with microporous and mesoporous characteristics are potential adsorbents for treating VOCs that are present in high-humidity and high-concentration streams. In the new adsorbent, spherical silica gel is used as a skeleton and biomass sugar is used as a suitable carbon source that is introduced to the silica gel channel via hydrothermal carbonization. At high temperatures, silica gel complies with the biomass carbon microspheres, in the case of losing hydroxyl groups, which is favorable for the formation of biomass charcoal. The prepared carbon–silica material is an adsorbent that exhibits a graded pore morphology and has effective hydrophobic properties. Moreover, it has good application prospects due to its excellent adsorption and desorption during VOC removal.

Acknowledgments

This work was supported by the Natural Science Foundation of China (Nos. 21506194 and 21676255) and Zhejiang Provincial Natural Science Foundation of China (Nos. Y14E080008 and Y16B070025).

Appendix A. Supplementary data

Supplementary data to this article can be found online at https://doi.org/10.1016/j.jes.2019.05.003.

REFERENCES

Balan, L., de Córdoba, M.C.F., Zaier, M., Ania, C.O., 2017. A green and fast approach to nanoporous carbons with tuned porosity: UV-assisted condensation of organic compounds at room temperature. Carbon 116, 264–274.

Böhme, K., Einicke, W.D., Klepel, O., 2005. Templated synthesis of mesoporous carbon from sucrose-the way from the silica pore filling to the carbon material. Carbon 43 (9), 1918–1925.

Cavaliere, P., Jahantigh, F., Shabani, A., Sadeghi, B., 2018. Influence of SiO_2 nanoparticles on the microstructure and mechanical properties of Al matrix nanocomposites fabricated by spark plasma sintering. Compos. Part. B-Eng. 146, 60–68.

Chen, X.W., Chong, J.J.E., Fah, Z.W.C., Hong, L., 2017. Glucose-derived carbon molecular sieve membrane: an inspiration from cooking. Carbon 111, 334–337.

Chu, L.L., Deng, S.W., Zhao, R.S., Zhang, Z., Li, C., Kang, X.J., 2015. Adsorption/desorption performance of volatile organic compounds on electrospun nanofibers. RSC Adv. 5 (124), 102625–102632.

Chu, L.L., Deng, S.W., Zhao, R.S., Deng, J.J., Kang, X.J., 2016. Comparison of adsorption/desorption of volatile organic compounds (VOCs) on electrospun nanofibers with Tenax TA for potential application in sampling. PLoS One 11 (10), e0163388.

Cui, J.L., Cheng, F.P., Lin, J., Yang, J.C., Jiang, K., Wen, Z.S., et al., 2017. High surface area C/SiO_2 composites from rice husks as a high-performance anode for lithium ion batteries. Powder. Technol. 311, 1–8.

Dou, B.J., Li, J.J., Wang, Y.F., Wang, H.L., Ma, C.Y., Hao, Z.P., 2011. Adsorption and desorption performance of benzene over hierarchically structured carbon–silica aerogel composites. J. Hazard. Mater. 196, 194–200.

Giraudet, S., Pré, P., Tezel, H., Le Cloirec, P., 2006. Estimation of adsorption energies using the physical characteristics of activated carbons and the molecular properties of volatile organic compounds. Carbon 44 (12), 2413–2421.

Gong, D.D., Li, S.S., Guo, S.X., Tang, H.G., Wang, H., Liu, Y., 2018. Lanthanum and cerium co-modified Ni/SiO_2 catalyst for CO methanation from syngas. Appl. Surf. Sci. 434, 351–364.

Hu, X.Y., Kang, X.R., Chen, T., Yan, X.L., Zhou, M., Komarneni, S., 2016. Facile synthesis of nanostructured porous carbon/silica composite and its adsorption property. J. Porous. Mater. 23, 833–836.

Kamal, M.S., Razzak, S.A., Hossain, M.M., 2016. Catalytic oxidation of volatile organic compounds (VOCs) - a review. Atmos. Environ. 140, 117–134.

Kiciński, W., Dembinska, B., Norek, M., Budner, B., Polanski, M., Kulesza, P.J., et al., 2017. Heterogeneous iron-containing carbon gels as catalysts for oxygen electroreduction: multi-functional role of sulfur in the formation of efficient systems. Carbon 116, 655–669.

Kuntasal, O.O., Karman, D., Wang, D., Tuncel, S.G., Tuncel, G., 2005. Determination of volatile organic compounds in different microenvironments by multibed adsorption and short-path thermal desorption followed by gas chromatographic-mass spectrometric analysis. J. Chromatogr. A 1099 (1–2), 43–54.

Liu, F., Dai, Y.X., Zhang, S., Li, J.M., Zhao, C.C., Wang, Y.Q., et al., 2018. Modification and application of mesoporous carbon adsorbent for removal of endocrine disruptor bisphenol a in aqueous solutions. J. Mater. Sci. 53 (4), 2337–2350.

Lu, H.F., Cao, J.J., Zhou, Y., Zhan, D.L., Chen, Y.F., 2013. Novel hydrophobic PDVB/R-SiO_2 for adsorption of volatile organic compounds from highly humid gas stream. J. Hazard. Mater. 262, 83–90.

Lu, J.X., Luo, M., Yakobson, B.I., 2017. Glass composites reinforced with silicon-doped carbon nanotubes. Carbon 128, 231–236.

Ojha, D.P., Song, J.H., Kim, H.J., 2019. Facile synthesis of graphitic carbon-nitride supported antimony-doped tin oxide nanocomposite and its application for the adsorption of volatile organic compounds. J. Environ. Sci. 79, 35–42.

Qiu, W.J., Dou, K., Zhou, Y., Huang, H.F., Chen, Y.F., Lu, H.F., 2018. Hierarchical pore structure of activated carbon fabricated by CO_2/microwave for volatile organic compounds adsorption. Chin. J. Chem. Eng. 26 (1), 81–88.

Twumasi, E., Forslund, M., Norberg, P., Sjostrom, C., 2012. Carbon–silica composites prepared by the precipitation method. Effect of the synthesis parameters on textural characteristics and toluene dynamic adsorption. J. Porous. Mater. 19, 333–343.

Wan, Y., Min, Y.L., Yu, S.H., 2008. Synthesis of silica/carbon-encapsulated core–shell spheres: templates for other unique core–shell structures and applications in in situ loading of noble-metal nanoparticles. Langmuir 24 (9), 5024–5028.

Wang, H.N., Tang, M., Zhang, K., Cai, D.F., Huang, W.Q., Chen, R.Y., et al., 2014a. Functionalized hollow siliceous spheres for VOCs removal with high efficiency and stability. J. Hazard. Mater. 268, 115–123.

Wang, H.Y., Zhu, T.L., Fan, X., Na, H.B., 2014b. Adsorption and desorption of small molecule volatile organic compounds over carbide-derived carbon. Carbon 67, 712–720.

Wang, H.N., Wang, T., Yu, M.H., Huang, X.D., Zhong, J., Huang, W. Q., et al., 2016a. Elaborate control over the morphology and pore structure of porous silicas for VOCs removal with high efficiency and stability. Adsorption 23 (1), 37–50.

Wang, R.X., Xie, M.N., Wang, H.J., Shi, X.H., Lei, C.P., 2016b. Adsorption properties of silica surface-grafted with a salicylhydroxamic acid-functionalized polymer toward lead ions. Korean J. Chem. Eng. 33 (3), 976–985.

Wang, C.C., Yang, S.D., Ma, Q., Jia, X., Ma, P.C., 2017. Preparation of carbon nanotubes/graphene hybrid aerogel and its application for the adsorption of organic compounds. Carbon 118, 765–771.

Yao, Y., Zhang, J.J., Xue, L.G., Huang, T., Yu, A.S., 2011. Carbon-coated SiO_2 nanoparticles as anode material for lithium ion batteries. J. Power. Source. 196, 10240–10243.

Yi, F.Y., Lin, X.D., Chen, S.X., Wei, X.Q., 2009. Adsorption of VOC on modified activated carbon fiber. J. Porous. Mater. 16 (5), 521–526.

Yu, X.Y., Wang, S.H., Zhang, J., 2018. Preparation of high adsorption performance activated carbon by pyrolysis of waste polyester fabric. J. Mater. Sci. 53 (7), 5458–5466.

Zaitan, H., Mohamed, E.F., Valdés, H., Nawdali, M., Rafqah, S., Manero, M.H., 2016. Toluene, methanol and benzaldehyde removal from gas streams by adsorption onto natural clay and Faujasite-Y type zeolite. Acta Chim. Slov. 63 (4), 798–808.

Zhang, D.D., Cao, J., Wu, G.P., Cui, L.Z., 2018. Dynamic adsorption model fitting studies of typical VOCs using commercial activated carbon in a fixed bed. Water Air Soil Poll. 229 (6), 178.

Zhao, Z.X., Wang, S., Yang, Y., Li, X.M., Li, J., Li, Z., 2015. Competitive adsorption and selectivity of benzene and water vapor on the microporous metal organic frameworks (HKUST-1). Chem. Eng. J. 259, 79–89.

Zhao, H.Y., Lu, X.A., Wang, Y., Sun, B., Wu, X.H., Lu, H.F., 2017. Effects of additives on sucrose-derived activated carbon microspheres synthesized by hydrothermal carbonization. J. Mater. Sci. 52 (18), 10787–10799.